AIMS Bioengineering

AIMS Bioengineering, 9(4): 383–399.
DOI: doi/10.3934/bioeng.2022028
Received: 13 September 2022
Revised: 11 December 2022
Accepted: 23 December 2022
Published: 28 December 2022

http://www.aimspress.com/journal/Bioengineering

Research article

A micro-CT evaluation of bone density around two different types of surfaces on one-piece fixo implants with early loading-an experimental study in dogs at 3 months

Jose Luis Calvo-Guirado[1,*], Nuria García Carrillo[2], Félix de Carlos-Villafranca[3], Miguel Angel Garces-Villala[4], Lanka Mahesh[5], Juan Carlos Ibanez[6] and Francisco Martinez-Martinez[7]

[1] Associate Researcher. Health Sciences Faculty.Universidad autónoma de Chile, 7500912, Chile, Private Practice Murcia, Spain
[2] Veterinarian, University of Murcia, Spain, 30007, Murcia, Spain
[3] Department of Orthodontics, Faculty of Medicine, University of Oviedo, Asturias, Spain
[4] Department of Implant and Biomaterial Research, Fundación Corazon de Jesus, San Juan, Argentin
[5] Private Practice New Delhi, India
[6] Director and Professor of the Career of Specialization in Oral Implantology at the Catholic University of Cordoba, Argentina
[7] Hospital Clinico Universitario Virgen de la Arrixaca, ctra, Madrid-Cartagena s/n, 30120, El Palmar, Murcia, Spain

* **Correspondence:** Email: jose.calvo@uautonoma.cl.

Abstract: The study's main objective was to evaluate the bone density and osseointegration around dental implants with two different implant surfaces with early loading, using a micro-CT device. Twenty-four Fixo® implants (Oxyimplant, Biomec Italy) 3.5 × 8.5 mm with Laser (test group) and acid-etched surface (control group) were placed in six young beagle dog's mandibles. MicroCT (Albira, Germay) evaluation with seven regions of interest was defined in each implant on two different surfaces. A total of 168 sites were studied, and four isocountours were also done in each implant at coronal, transversal, and sagittal scanned areas to evaluate bone density location. The effect on the bone evaluation of two different surfaces variables was evaluated at the mesial and distal positions, showing crestal, medial, and apical types of bone density. Implant positions (P2, P3, P4, and M1) were also analyzed to determine bone density areas. The results of hard tissue density indicated a statistical significance for laser surface at crestal ROIs level ($p < 0.001$) and position of implants ($p = 0.032$)

related to P3 areas compared to the acid-etched surface in Fixo® implants. Density D4 was the most common type of bone surrounding Fixo® standard implants at three different positions and density D3 was the most found on Fixo® laser surfaces. Micro-CT evaluation was a powerful tool for measuring the type of bone quality and location surrounding dental implants. Micro-CT study revealed that the most common density type found around Fixo® laser surface (test) implants was density D3 at the mesial and distal coronal part and density D4 at the middle and apical part. Fixo® implant with acid-etched surface showed the type of density D4 bone in hole implant at 3 months follow-up. It is a complementary histologic and histomorphometric analysis method for implant surrounding bone density.

Keywords: one-piece implants; fixo implants; laser surface; acid-etched surface; Hounsfield unit; micro-computed tomography; micro-CT

1. Introduction

Nowadays, to assess virtual biomechanics testing for dental implants approach is based on microcomputed tomography (micro-CT or μCT) data, providing noninvasive methods for determining trabecular and cortical bone stiffness and strength. Those virtual testing outcomes could be used to predict global elastic-plastic properties and may reduce the cost, time, and a number of test specimens in performing physical experiments [1]. Clinical practices have cone beam CBCT, which affords a more localized assessment of the maxillofacial region, including the dentition, reducing patient's X-ray exposure. As clinical use of CT technologies has grown over the past decade or more, so have the advancements in high-resolution micro-CT imaging for use in both primary and preclinical research settings [2]. Computed tomography (micro-CT) imaging is a ubiquitous, cost-effective, and noninvasive three-dimensional imaging modality advancements established that micro-CT imaging at the forefront of preclinical research, able to provide anatomical, functional, and even molecular information while serving as a testbench for translational research [3]. The design of an implant must have long threads with higher thread depth in the apical area for primary stability, a long furrow for bone debris, and a rough surface will improve osseointegration in immediate implantation. All these features are essential to increase the load transfer to cancellous bone and decrease load transfer to the crestal cortical bone [4–6]. The position of the implants plays a vital role in implants placed in a subcrestal position having less crestal bone resorption when compared with implants placed crestally [7–11]. The first microCT-based data of the zygomatic bone compared with the anterior and posterior maxilla in a Caucasian population was presented. The zygomatic trabecular bone quality was poor compared with the maxilla. The present intra-individual analysis proved a comparable trabecular bone quality of the zygomatic bone with the anterior maxilla [12]. Micro-CT already offers a powerful new tool for the 3D visualization and quantification of the canal network within human cortical bone [13]. One-piece implants as a single unit and monoblock with healing prosthetic parts manufactured as one unit are one of the most remarkable advantages offered by one-piece implants, immediate placement with immediate restoration brings patient satisfaction in the end [14,15]. Also, one-piece implant geometry may have an impact on marginal bone loss, related to geometric thread parameters establishment of a biologic width [9], vertical soft tissue thickness [16], implant positioning relative to the alveolar crest [11,17], implant collar design [8,18], smoke [19], and peri-implantitis [20,21]. In its different

forms, x-ray-based computed tomography (CT) represents the gold standard technology for the noninvasive imaging and quantification of mineralized tissues. Significant correlations were found between Hounsfield density obtained by computed tomography, and bone mass determined by micro-CT, but not with DXA values. Cortical thickness measurements correlated well with CT and micro-CT [22]. In clinical practice, CT remains the most appropriate routine for bone qualitative and quantitative evaluation at the mandible. This ex vivo study confirms that mandibular bone status does not reflect the axial skeletal one and assists in placing implants with dental prostheses in old or osteoporotic patients [22].

The evaluation of bone formation related to these implants was the CBTC, the only diagnostically justifiable imaging technique that allows approximate conclusions about the bone density surrounding implants. Bone density (BD) can be assessed using Hounsfield units (HU), which are directly related to the tissue attenuation coefficient [23]. Lopez-Valverde et al. evaluated surfaces coatings with chitosan or melatonin in peri-implant bone density with micro-CT evaluation, which proved to be a very useful method for the measurement of Bone density around the implants [24]. X-ray microtomography (microCT) is a conservative technique used to evaluate bone morphometry and bone quality, and several studies have demonstrated its usefulness in quantifying bone tissue [25,26]. Micro-CT was developed in the early 1980s with a high spatial resolution for smaller volumes than CT. voxels, making it possible to measure trabecular and cortical bone by assessing the qualitative and quantitative morphometry around dental implants [27,28]. Micro-CT compared with CBCT devices showed similar BvTv values with no statistical difference, showing that the CBCT device could assess trabecular bone with under or overestimated values compared to μCT [29].

The correlation between micro-CT and MSCT and multislice computed tomography (MSCT) suggested that bone density measurements could be used to estimate bone microstructural parameters in bone quality assessment at the implant site or in vivo studies [29–31]. Therefore, the main objective of our study is to establish a protocol for measuring the bone density around one type of implant with two different treatment surfaces and evaluate how crestal and subcrestal placement influences crestal bone loss obtained from the micro-CT evaluation in beagle dogs at three months follow-up.

2. Materials and methods

2.1. Material

Six Beagle dogs, approximately 1.5 years old and weighing between 12 and 14 kg, were used in this study. A total of 24 implants were inserted, four implants in each hemimandible, and the other hemimandible was left as natural healing. One-piece implants were randomly divided into laser surface (test group) and standard acid-etched surface (control group). The study was designed and conducted according to the "Guide for Care and Use of Laboratory Animals" (8^{th} ed) and European Directive 2010/63/E.U. (14). The project was approved by the University of Murcia's "Institutional Animal Care and Use Committee" (CEEA) in process number A1320141102. A veterinarian responsible for the study checked the dogs' health before starting the study. A housing time of 2 weeks was allowed before the surgical procedure. All animals presented an excellent general health status, without any systemic pathology, occlusal trauma, or fungal or viral lesions in the oral cavity. The animals were pre-anesthetized with acepromazine maleate 0.2%–1.5 ml/kg (Calmo-Neosan, Pfizer, Madrid) together with Buprenorphine, 12 μg/kg (Bupaq®, Richter Pharma AG, Oberoesterreich, Austria) and Atropine, 0.04

mg/kg intramuscular (Atropine-Zoo®, Zoo Lab. Bogota, Colombia). The drug mixture was injected intramuscularly into the quadriceps femoris. Immediately, the animals were taken to the surgical room and an intravenous catheter (diameter 22 or 20 G) was inserted in the cephalic vein, infusing Propofol® (Propovet, Abbott Laboratories Ltd. Queensborough, Kent, UK) at a rate of 0.4 mg/kg/min slowly and at a constant infusion rate. Anesthetic maintenance was performed using volatile anesthetics. In addition, local anesthesia (Articaine 40 mg, with 1% epinephrine, Ultracain®, Normon, Madrid, Spain) was administered at the surgical sites. All procedures were performed under the supervision of a veterinary surgeon. This technique was applied in all animal studies done at the University of Murcia by Calvo-Guirado et al. [8–11]. The implants used were one-piece called Fixo® 0° (Oxyimplant®, Biomec, Italy) (Figure 1).

Figure 1. Fixo one-piece implant 3.5Ø × 8.5 mm length 0°.

2.2. Methods

Extractions of premolars and mandibular first molar (P2, P3, P4, M1) were performed in the hole mandibular of each animal. Teeth were sectioned at the root bifurcation in the lingual vestibule direction with a tungsten carbide bur to extract the roots individually employing an elevator and forceps without damaging the bony walls. This procedure was applied in all animal studies done at the University of Murcia by Calvo-Guirado et al. in previous studies [8–11]. The placement of the Fixo® implants (Oxyimplant, Biomec, Colico, Lecco, Italy) was determined by the randomization program http://www.randomization.com, where the two different implant surfaces and two different positions were assigned to the experimental animals. The other hemimandible was used to place other types of implants from the same company, not evaluated in this study. The study's design planned 24 implants in the mandible: 12 implants coated with a new laser surface (test) and 12 with the acid-etched surface (control) one-piece called Fixo® 0°. Each dog received four one-piece implants (3.5Ø × 8.5 mm length, four per hemi-arch, randomly assigned in the mandible. Before implant placement, the vestibular,

lingual, mesial, and distal dimensions of the entrance of the fresh extraction sockets were measured with a sliding caliper, determining the measurements of the medial alveolar ridge (Figure 2).

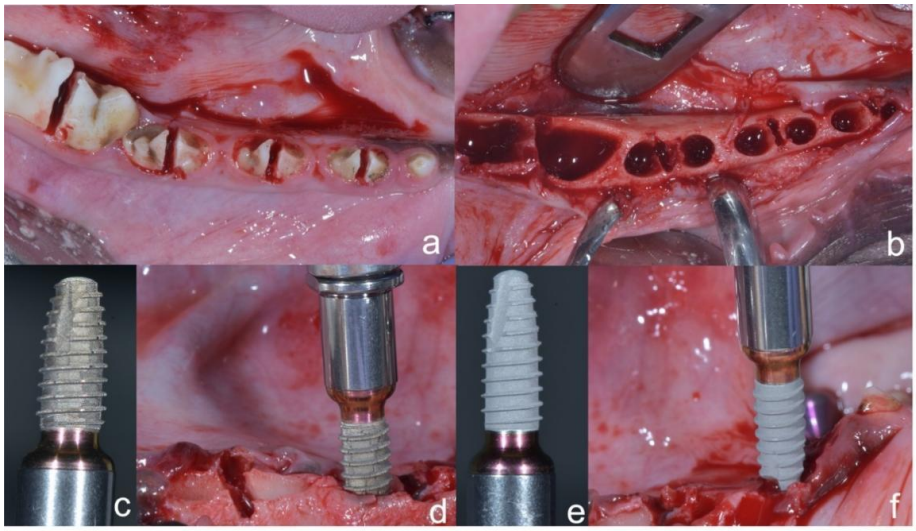

Figure 2. (a) Odontosection of premolars and molar teeth. (b) empty sockets of extraction roots. (c) Fixo® implant with rough laser surface. (d) Laser Fixo® implants inserted in alveolar sockets. (e) Fixo® acid-etched surface. (f) Fixo® acid-etched surface inserting in alveolar sockets.

After implants were placed, implant stability was measured with Ostell Mentor® (Stampgatan, Goteborg, Sweden) which evaluates the primary stability by radiofrequency analysis (RFA) using ISQ (implant stability quotient) values (Figure 3).

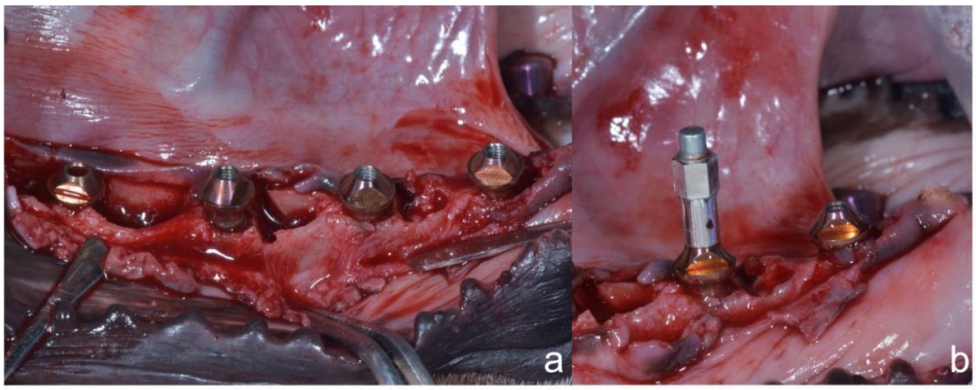

Figure 3. (a) Fixo® implants placed crestally and subcrestally related to buccal bone plate. (b) Ostell smart peg in place.

On the other hand, after we placed the healing screw and the stitches were done, the other method to evaluate implant stability is the Periotest device (Medizintechnik Gulden, Modautal, Germany) (Figure 4).

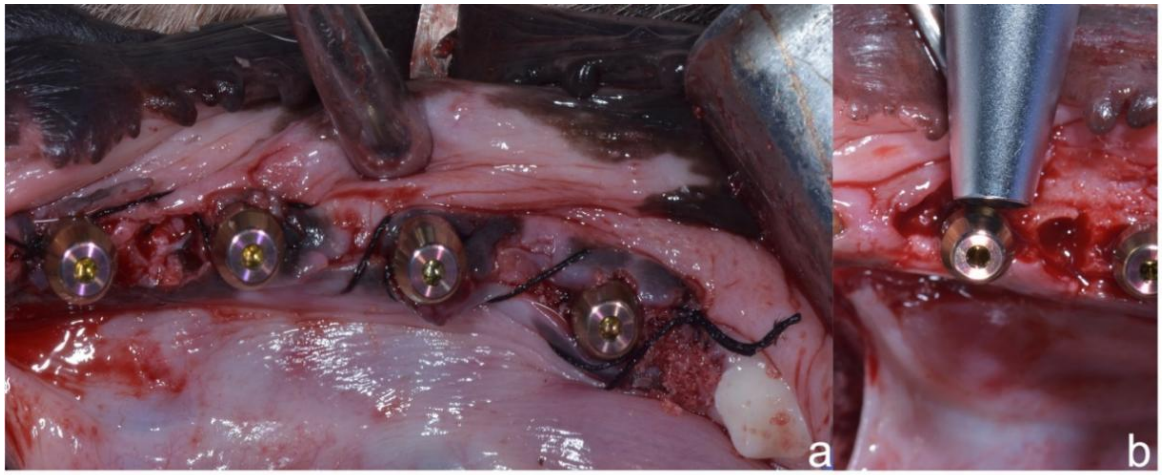

Figure 4. (a) Fixo implants placed with healing screws. (b) Periotest device evaluating implant stability.

Flaps were closed using simple non-absorbable interrupted sutures (Silk 3–0®, Lorca Marin, Lorca, Spain). After the surgical procedures, the animals received antibiotics twice daily (Amoxicillin 500 mg, Clamoxyl® L.A., Pfizer, Madrid, Spain) and analgesics three times a day (Ibuprofen 600 mg, Rimadyl®, Pfizer, Madrid, Spain). Sutures were removed after seven days. The animals had free access to water and were fed wet balanced dog food for 7 days after surgery. All dogs were sacrificed 12 weeks after implant placement using pentothal natrium (Abbot Laboratories, Madrid, Spain) perfused through the carotid arteries with a fixative containing a mixture of 5% glutaraldehyde and 4% formalin. The jaws were dissected, and block sections, including the implant sites and the surrounding soft and hard tissues, were removed with a saw. This procedure was applied in all animal studies done at the University of Murcia by Calvo-Guirado et al. in previous studies [8–11]. Micro-computed tomography analysis. The sections of the block, including the segments with implants, were preserved and fixed in 10% neutral formalin. Image acquisitions were performed using a multimodal PET/SPECT/CT Albira II ARS scanner (Bruker® Corporation, Karlsruhe, Germany) belonging to the University of Murcia. The acquisition parameters were 45 Kv, 0.2 mA, and 0.05 mm voxel. The acquisition slices were axial, 0.05 mm thick, and 800 to 1000 images were obtained from each piece through a flat-panel digital detector with 2400 × 2400 pixels, and a FOV (Field of View) of 70 × 70 mm^2 was used to capture 600 voxel projections of 0.125 mm^3. Scanner exposure per block was 15–20 min. The approximate radiation deep dose equivalent for CT (computed tomography) settings was 226 millisievert (mSV), and the shallow dose equivalent was 358.9 mSV (Figure 5).

The implants were grouped according to the three axes (transverse, coronal, and sagittal), to check the image in the sagittal section. In all the images, the same parameters in FOV (%): 90 and zoom: 0.5 and with a hardness of bone density around the implant were quantified in Hounsfield units (HU), using seven 1 × 1 mm squares or regions of interest (ROI) in the BIC (bone-to-implant contact) area, two in the crestal area, two in the medial, two in the apical area, and one in the tip of the implant, using a medical image data examiner (Figure 6).

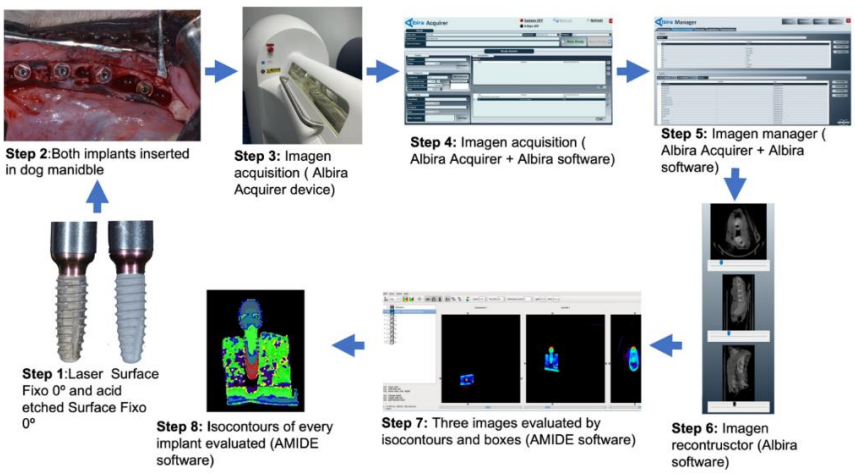

Figure 5. Technical of different steps followed for the acquisition and processing of the micro-CT image in crushed teeth. Step 1: Laser and acid-etched surface fixo implants. Step 2: Fixo implants inserted in the mandible. Step 3: Imagen acquisition (Albira Acquirer device). Step 4: Imagen acquisition (Albira Acquirer + Albira software). Step 5: Imagen manager (Albira Acquirer + Albira software). Step 6: Imagen reconstructor (Albira software). Step 7: Segmentation and quantification (Amide). Step 8: Isocontours evaluated by AMIDE software.

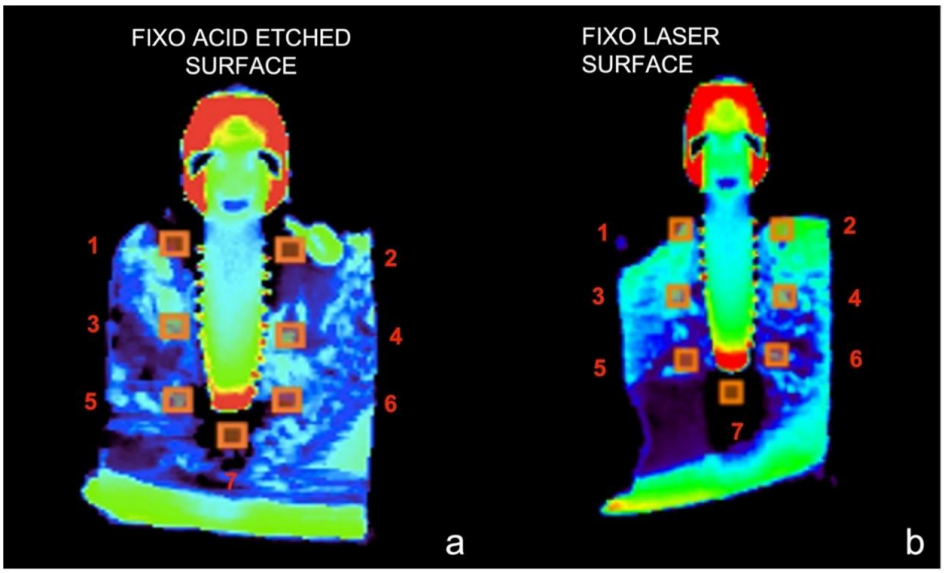

Figure 6. Bone density boxes in different areas marked in orange. (a) Fixo acid-etched surface. (b) Fixo laser surface. Two boxes marked on mesial and distal crestal bone (1 and 2), two boxes in the middle of the implant body (3 and 4), two boxes in the apical area (5 and 6), and one in the tip of the implant (7).

Regions of interest (ROI) were defined as the peri-implant bone covering the implant surface with different isocontours (manual measurement done in AMIDE software) according to the three axes (transverse, coronal, and sagittal) to determine the type of bone obtained by AMIDE software. The

software for viewing, analyzing, and registering volumetric medical imaging data sets (AMIDE, UCLA University, LA, USA) (Figures 7 and 8).

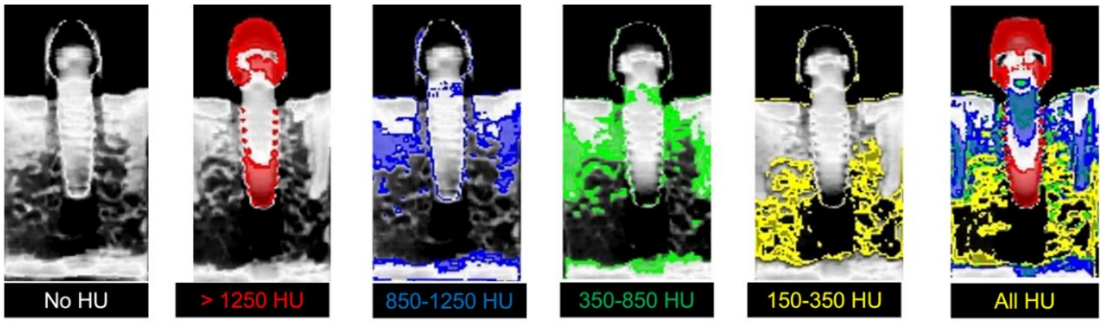

Figure 7. Isocontour of all measurements. Yellow color 150–350 HU (Quality D4), green color 350–850 HU (Quality D3), blue color 850–1250 HU (Quality D2), and red color > 1250 HU (similar to Quality D1) (AMIDE images).

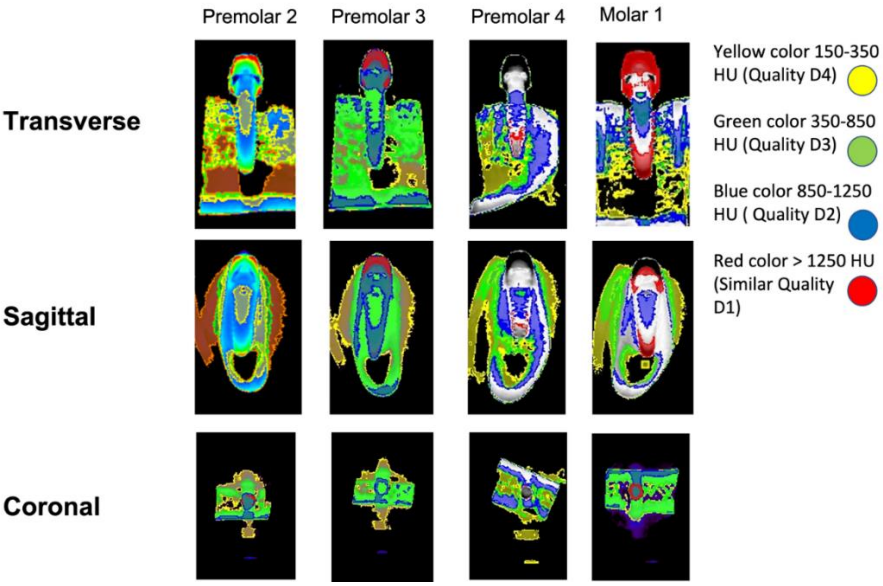

Figure 8. Isocontours of all measurements in all teeth areas. Yellow color 150–350 HU (Quality D4), green color 350–850 HU (Quality D3), blue color 850–1250 HU (Quality D2), and red color > 1250 HU (similar to Quality D1) (AMIDE images).

2.3. Statistical Analysis

Descriptive analysis was performed with statistical package for social science (SPSS for Windows version 15.0). The statistical power obtained evaluated 168 box locations in 24 implants placed in 6 hemimandible dogs (7 of each implant) and four isocontours. Bone density variables were analyzed in crestal, mid, and apical areas. These sample sizes allow, using the t-test for independent groups and with a power of 80% and 6% alpha error, the detection of an estimated Cohen's d of 0.45 (below a medium effect size according to Cohen's scale when comparing HU measurements between two

groups). The results are expressed as mean ± S.D. Differences between groups related to the surface in each density range (HU) were analyzed by Student's t-test and Tukey's post hoc test. Differences were considered statistically significant when $p < 0.05$.

3. Results

MicroCT evaluation was done with the data of the mean of Hounsfield units obtained around the hole one-piece implant. The results obtained comparing Laser and acid-etched surfaces ROIs values were fixo laser surface 540.14 ± 0.23 Hounsfield units (HU), and fixo acid-etched surface was 516.22 ± 0.22 HU. This means that the laser surface got more new bone around the implants compared with the standard acid-etched surface (Figure 9). The results mean that the Laser surface treatment has more clot retention and quick bone formation around fixo implants from the middle to the crestal part of the implant. The acid-etched surface, which is the commercial surface of fixo implants, demonstrated that the bone formation around the implants gets solid and stable at three months of healing.

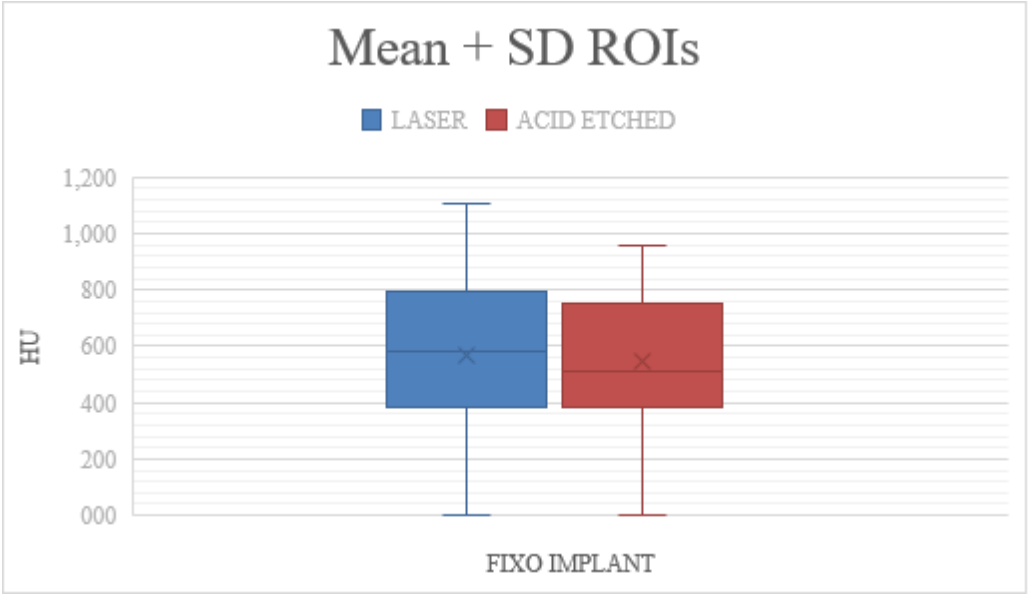

Figure 9. Evaluation of two different surfaces comparison ROIs.

Periotest values (PTV) were at the day of implant placement with the Laser surface −6.79 ± 0.31, significantly higher compared with the acid-etched surface in acid-etched surface −4.33 ± 0.54. The same values were obtained at three months with a laser surface of −7.79 ± 0.45* compared with an acid-etched surface of −5.83 ± 0.29 (Table 1).

Table 1. Comparison of Periotest® (PT) values between groups (*$p < 0.05$).

PT values	Day 0	1 Month	3 Month
Acid etched surface	−4.33 ± 0.54	−4.18 ± 0.33	−5.83 ± 0.29
Laser surface	−6.79 ± 0.31*	−6.22 ± 0.39*	−7.79 ± 0.45*

The most predictable data obtained by our study was the clinical one when we inserted the implants and when we finished the study the implant stability quotient (ISQ) was at the day of implant placement with Laser surface 76.17 ± 2.56* significantly higher compared with the acid-etched surface in acid-etched surface 73.65 ± 0.13. The same values were obtained at three months with a laser surface of 77.66 ± 1.34* compared with an acid-etched surface of 75.89 ± 2.45 (Table 2). Those results meant that Laser surface stimulates new bone formation quicker than a conventional acid-etched surface at one and three months of follow-up.

Table 2. Comparison of Ostell Mentor® (ISQ) values between groups (*$p < 0.05$).

ISQ values	Day 0	1 Month	3 Month
Acid etched surface	73.65 ± 0.13	70.56 ± 2.87	75.89 ± 2.45
Laser surface	76.17 ± 2.56*	71.22± 0.88	77.66 ± 1.34*

Micro-CT evaluation showed that fixo laser surface implants subcrestally placed (test group) have high bone formation at three months compared with fixo acid-etched implants. Density D3 and D4 were found more in test implants at mesial and distal crestal placement than those with the standard surface. The type of bone density D2 was found more in boxes in both surfaces' middle of the implant body. The type of bone density D1 was as more than 1250 HU, was not found, but the titanium implant has this density reaching 1250 HU. D2 density, which is a bone with thick cortical and thick marrow bone from 850 to 1250 HU, has been found more in fixo implants with laser surface in the middle of body implant areas than fixo with the standard surface. D3 density, reached from 350 to 850 HU, has been found in both groups of implants. The most common quality of bone was D3 bone, from 150 to 350 HU, found in all implant areas and the same quantity in both implant groups (Figure 10). Our results mean that the new bone formation around dental implants at three months in the dogs is deficient, increasing in time, but we need more time for surrounding implant bone stiffness. Bone remodeling around implants should be achieve after six months following our results.

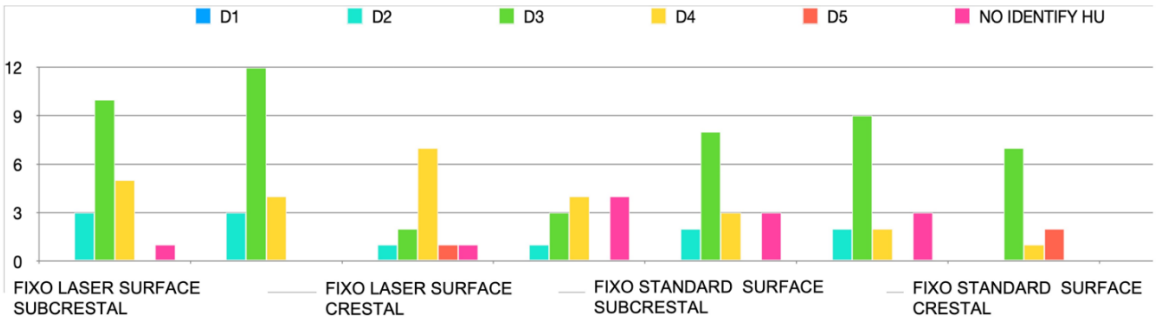

Figure 10. Evaluation of two different surfaces in the same implant design. D3 density was the most common type of bone found around both implant surfaces, with a significant increase in fixo laser implants.

The total sample consisted of 168 sites (ROIs). A similar bone density range was observed in the different ROIs, depending on their location or level (crestal, medial, and apical) and implant position

(P2, P3, P4, and M1). Regarding surface coating, the highest bone density (+ 950 Hounsfield units) was recorded in the medial of left M1, in laser surface, with mean values of 0.80 ± 0.23 and for the acid-etched area was 0.61 ± 0.11, respectively, and the lowest BD (bone density) was recorded in the apical area (−250 Hounsfield units) were obtained in apical area could be explained by the proximity of the dental nerve canal in this region. Regarding implant position, the highest BD (bone density) (+ 950 Hounsfield units) was recorded in all implant M1 and the lowest (−150 Hounsfield units) in P2. Mean values and standard deviations showed in Table 3 and 4.

Table 3. The mean and standard deviation of all implant areas were taken. With procedure regress in SUDAAN to account for clustering (multiple sites within teeth). Procedure DESCRIPT in SUDAAN, where *p < 0.05.

Variable	N	Acid etched surface	Laser surface	P value global
Implant area		Mean ± SD	Mean ± SD	
All ROIs	168	0.39 ± 0.32	0.57 ± 0.45*	0.002
Crestal (C)	56	0.61 ± 0.11	0.80 ± 0.23	0.762
Middle (M)	56	0.46 ± 0.34	0.49 ± 1.22	0.689
Apical (A)	56	−0.28 ± 0.14	−0.15 ± 0.55	0.543
P value		< 0.003	< 0.003	–
Surface comparisons		C vs M vs A	C vs M vs A	

Table 4. The mean and standard deviation of all implant positions were taken. With procedure REGRESS in SUDAAN to account for clustering (multiple sites within teeth). Procedure DESCRIPT in SUDAAN, where *means p < 0.05.

Variable	N	Acid etched surface	Laser surface	P value global
Implant position		Mean ± SD	Mean ± SD	
All ROIs	168	0.39 ± 0.32	0.57 ± 0.45*	0.003
M1	42	0.09 ± 0.18	0.07 ± 0.33	0.421
P4	42	0.18 ± 0.22	0.19 ± 0.22	0.764
P3	42	0.16 ± 0.38	0.18 ± 0.38	0.558
P2	42	0.16 ± 0.39	0.18 ± 0.39	0.652
P value		< 0.003	< 0.003	
Site comparisons		P2 vs P3 vs P4 vs M1	P2 vs P3 vs P4 vs M1	

4. Discussion

This study aimed to evaluate the bone density around laser surface dental implants and compared it with conventional acid-etched surface implants with micro-CT, after 12 weeks of immediate post-extraction placement, in the jaws of Beagle dogs. Early loading in edentulous mandibles seems justified in cases with good implant primary stability Calvo-Guirado et al. stated that the immediate loading related to several factors such as bone relaxation following compression, biological changes associated with early bone healing, initiation of marginal bone resorption, and immediate loading conditions [32,33]. Micro-CT has proven to be a suitable technique for assessing bone quality and quantity in animal models, it is also a valuable tool for evaluating human biopsies and necropsies, having been used not only qualitatively but also quantitatively in different clinical situations [34–36]. It is a noninvasive diagnostic tool that allows the use of samples for other types of measurements and is also of great interest in the clinic, where, for obvious reasons, conventional histomorphometry cannot be performed [37]. Micro-CT can be used to evaluate the morphometric characteristics as a complementary alternative to conventional histological and histomorphometric analysis [38]. In addition, it is an accurate and time-saving technique for determining bone morphometry compared to manual methods [39–41]. In our research, measurements of Hounsfield units ranged from 330 to 995 when all 168 sites were evaluated 12 weeks after implantation. A total of 168 sites were analyzed for the three surfaces studied in the crestal, medial, and apical levels (ROIs) and at the implant locations (P2, P3, P4, and M1). In the Norton and Gamble study [42], taken as a reference, a single standard implant of Ø3.5 mm × 11 mm length was used to allow the software to calculate the bone density values and, in our study, the implants used were Ø3.5 mm × 8.5 mm. The results of our study provided valuable information on different coatings of dental implants to achieve better and faster osseointegration: the surfaces treated with Laser showed similar bone density values around the implants to the control surface. The most validated strategy to improve the bone-implant interface continues to be the modification of the surface topography by increasing macro-, micro, and nano-roughness [43]. On the other hand, to improve the bioactivity of implants, some studies have proposed surface modification by incorporating organic and inorganic ions and molecules, proteins, enzymes, and pharmaceuticals, on the Titanium oxide layer (TiO2). In this regard, combining organic and inorganic components in Titanium surface re-coatings would lead to bone-like coatings improving the functionality and biological efficacy [43,44]. Another finding of our study was the statistical significance we found for bone density in different levels (crestal, medial, and apical) ($p < 0.001$) and positions (P2, P3, P4, and M1) ($p = 0.032$) of the implants. In this regard, our results agreed with Chavez et al. [45] who, in their respective studies in mandibles, found significant variations in bone density within the mandible, which would underline the importance of identifying specific locations before implant placement. We also found that micro-CT was a beneficial diagnostic method for measuring peri-implant BD measured in HU. This parameter is a key factor to consider when predicting implant stability and survival. This survival is conditioned by bone quality, i.e., bone density around implants is decisive for their osseointegration [45,46]. However, our study's results showed several limitations that we describe below, agreeing with Barret and Smet et al., when defining an ROI in a micro-CT image. In this study, we draw ROIs at a "safe" distance from the implant in cross-sections, but, despite this, an image may be distorted by metallic scatter, and certain studies have highlighted the difficulty in performing an accurate morphometric analysis of the bony areas surrounding an implant [47,48]. Rebaudi et al. reported that these artifacts created in the areas close to

the implant would lead to biases in the measurement of bone density in these areas [49,50]. In the same experimental study in dogs, Song et al. demonstrated that 45 to 63 mm was a reasonable distance to compensate for artifacts in bone morphometric analysis of an implant containing the tissue sample assessed by micro-CT, and the acquisition distance in our study far exceeded this figure [51]. In a resume, micro-CT techniques are used to quantify peri-implant BD do not provide specific histological information on the nature of the bone formed around the surfaces tested, despite the color coding of the HU provided by the AMIDE software. Regarding clinical applicability, micro-CT imaging at the forefront of preclinical research can provide the quality and quantity of our bone, and it will be helpful to provide the quality and density around Osseointegrated implants. Micro CT has become an essential tool for analyzing mineralized tissues, increasing transparency and reproducibility, promoting best practices, and providing a basic framework to apply μCT analysis to the dentoalveolar complex in humans.

5. Conclusions

Based on the experimental study, fixo implants with laser surface showed less marginal bone loss compared to control group implants placed at subcrestal level after Micro CT evaluation at three months follow-up. Micro CT revealed that the most common density type found around fixo laser surface implants was density D3 at the mesial and distal coronal part and density D4 at the middle and apical part. Fixo acid-etched surface showed the type of bone density D4 bone in hole implant at three months follow-up. We need the histological evaluation to compare the type of bone and bone-to-implant contact to confirm our micro-CT results, but it is a complementary method for histologic and histomorphometric analysis for implant surrounding bone density.

Acknowledgments

We would like to thank the companies Biomec SL (Italy) and MADIMPLANT (Madrid, Spain), Olivio Dela Bella and Eduardo Izquierdo, who provided the material for its development and research.

Conflict of interest

The authors declare no conflict of interest.

Author contributions

Conceptualization, Jose Luis Calvo-Guirado, Francisco Martinez-Martinez; data curation Mari Carmen Gonzalez Escudero, Nuria Garcia Carrillo, formal analysis Felix de Carlos-Villafranca, Miguel Angel Garces-Villala, funding acquisition, Jose Luis Calvo-Guirado, Francisco Martinez-Martinez; investigation Jose Luis Calvo-Guirado, Mari Carmen González Escudero, Nuria Garcia Carrillo, methodology, Francisco Martinez-Martínez, Felix de Carlos-Villafranca, project administration Jose Luis Calvo-Guirado, resources Francisco Martinez-Martinez; software, Felix de Carlos-Villafranca, Miguel Angel Garces-Villala, supervision Jose Luis Calvo-Guirado, Francisco Martinez-Martinez; validation, Mari Carmen Gonzalez Escudero, Nuria Garcia Carrillo, visualization Jose Luis Calvo-Guirado; writing-original draft preparation, Jose Luis Calvo-Guirado, Francisco Martinez-Martinez; writing-review and editing. Jose Luis Calvo-Guirado, Felix de Carlos-Villafranca,

Nuria Garcia Carrillo, Francisco Martinez-Martinez; translations and final corrections; Lanka Mahesh, Juan Carlos Ibanez.

References

1. Ramezanzadehkoldeh M and Skallerud BH (2017) MicroCT-based finite element models as a tool for virtual testing of cortical bone. *Med Eng Phys* 46: 12–20. https://doi.org/10.1016/j.medengphy.2017.04.011
2. Cox TC (2020) Microcomputed tomography of craniofacial mineralized tissue: a practical user's guide to study planning and generating quality data. *Bone* 137: 115408. https://doi.org/10.1016/j.bone.2020.115408
3. Clark DP and Badea CT (2021) Advances in micro-CT imaging of small animals. *Phys Med* 88: 175–192. https://doi.org/10.1016/j.ejmp.2021.07.005
4. Ormianer Z, Matalon S, Block J, et al. (2016) Dental implant thread design and the consequences on long-term marginal bone loss. *Implant Dent* 25: 471–477. https://doi.org/10.1097/ID.0000000000000441
5. Abuhussein H, Pagni G, Rebaudi A, et al. (2010) The effect of thread pattern upon implant osseointegration. *Clin Oral Implants Res* 21: 129–136. https://doi.org/10.1111/j.1600-0501.2009.01800.x
6. El-Gammal M, Ghoneem N, Tawfik H, et al. (2014) Early-loaded laser-sintered versus acid-etched one-piece dental implants for mandibular premolars replacement: a preliminary study. *Implant Dent* 23: 565–569. https://doi.org/10.1097/ID.0000000000000133
7. Valles C, Rodriguez-Ciurana X, Clementini M, et al. (2018) Influence of subcrestal implant placement compared with equicrestal position on the peri-implant hard and soft tissues around platform-switched implants: a systematic review and meta-analysis. *Clin Oral Invest* 22: 555–570. https://doi.org/10.1007/s00784-017-2301-1
8. Calvo-Guirado JL, Lopez-Lopez PJ, Mate Sanchez JE, et al. (2014) Crestal bone loss related to immediate implants in crestal and subcrestal position: a pilot study in dogs. *Clin Oral Implants Res* 25: 1286–1294. https://doi.org/10.1111/clr.12267
9. Negri B, Lopez Mari M, Mate Sanchez de Val JE, et al. (2015) Biological width formation to immediate implants placed at different level in relation to the crestal bone: an experimental study in dogs. *Clin Oral Implants Res* 26: 788–98. https://doi.org/10.1111/clr.12345
10. Perez-Albacete Martinez C, Vlahovic Z, Scepanovic M, et al. (2016) Submerged flapless technique vs. conventional flap approach for implant placement: experimental domestic pig study with 12-month follow-up. *Clin Oral Implants Res* 27: 964–968. https://doi.org/10.1111/clr.12665
11. Calvo-Guirado JL, Gomez-Moreno G, Delgado-Ruiz RA, et al. (2014) Clinical and radiographic evaluation of osseotite-expanded platform implants related to crestal bone loss: a 10-year study. *Clin Oral Implants Res* 25: 352–358. https://doi.org/10.1111/clr.12134
12. Bertl K, Heimel P, Rokl-Riegler M, et al. (2015) MicroCT-based evaluation of the trabecular bone quality of different implant anchorage sites for masticatory rehabilitation of the maxilla. *J Craniomaxillofac Surg* 43: 961–968. https://doi.org/10.1016/j.jcms.2015.04.008
13. Cooper D, Turinsky A, Sensen C, et al. (2007) Effect of voxel size on 3D micro-CT analysis of cortical bone porosity. *Calcif Tissue Int* 80: 211–219. https://doi.org/10.1007/s00223-005-0274-6

14. Ghaleh Golab K, Balouch A, Mirtorabi S (2016) One-year multicenter prospective evaluation of survival rates and bone resorption in one-piece implants. *Clin Implant Dent Relat* Res 18: 392–400. https://doi.org/10.1111/cid.12299
15. Duda M, Matalon S, Lewinstein I, et al. (2016) One piece immediately loaded implants versus 1 piece or 2 pieces delayed: 3 years outcome. *Implant Dent* 25: 109–113. https://doi.org/10.1097/ID.0000000000000343
16. Rodriguez-Ciurana X, Vela-Nebot X, Segala-Torres M, et al. (2009) The effect of interimplant distance on the height of the interimplant bone crest when using platform-switched implants. *Int J Periodontics Restorative Dent* 29: 141–151. https://pubmed.ncbi.nlm.nih.gov/19408476
17. Kadkhodazadeh M, Safi Y, Moeintaghavi A, et al. (2019) Marginal bone loss around one-piece implants: a 10-year radiological and clinical follow-up evaluation. *Implant Dent* 28: 237–243. https://doi.org/10.1097/ID.0000000000000861
18. Linkevicius T, Apse P, Grybauskas S, et al. (2009) The influence of soft tissue thickness on crestal bone changes around implants: a 1-year prospective controlled clinical trial. *Int J Oral Maxillofac Implants* 24: 712–719. https://pubmed.ncbi.nlm.nih.gov/19885413
19. Clementini M, Rossetti PH, Penarrocha D, et al. (2014) Systemic risk factors for peri-implant bone loss: a systematic review and meta-analysis. *Int J Oral Maxillofac Surg* 43: 323–334. https://doi.org/10.1016/j.ijom.2013.11.012
20. Romanos GE, Javed F, Delgado-Ruiz RA, et al. (2015) Peri-implant diseases: a review of treatment interventions. *Dent Clin North Am* 59: 157–178. https://doi.org/10.1016/j.cden.2014.08.002
21. Fickl S, Kebschull M, Calvo-Guirado JL, et al. (2015) Experimental peri-implantitis around different types of implants-a clinical and radiographic study in dogs. *Clin Implant Dent Relat Res* 17: e661–669. https://doi.org/10.1111/cid.12303
22. Bodic F, Amouriq Y, Gayet-Delacroix M, et al. (2012) Relationships between bone mass and micro-architecture at the mandible and iliac bone in edentulous subjects: a dual X-ray absorptiometry, computerised tomography and microcomputed tomography study. *Gerodontology* 29: e585–594. https://doi.org/10.1111/j.1741-2358.2011.00527.x
23. Hounsfield, G.N. (1973) Computerized transverse axial scanning (tomography): description of system. *Br J Radiol* 46: 1016–1022. https://doi.org/10.1259/0007-1285-46-552-1016
24. Lopez-Valverde N, Lopez-Valverde A, Aragoneses JM, et al. (2021) Bone density around titanium dental implants coating tested/coated with chitosan or melatonin: an evaluation via microtomography in jaws of Beagle dogs. *Coatings* 11: 777. https://doi.org/10.3390/coatings110707
25. Irie MS, Rabelo G, Spin-Neto R, et al. (2018) Use of micro-computed tomography for bone evaluation in dentistry. *Braz Dent J* 29: 227–238. https://doi.org/10.1590/0103-6440201801979
26. Peyrin F (2011) Evaluation of bone scaffolds by micro-CT. *Osteoporos Int* 22: 2043–2048. https://doi.org/10.1007/s00198-011-1609-y
27. Young S, Kretlow JD, Nguyen C, et al. (2008) Microcomputed tomography characterization of neovascularization in bone tissue engineering applications. *Tissue Eng Part B Rev* 14: 295–306. https://doi.org/10.1089/ten.teb.2008.0153
28. Swain M and Xue J (2009) State of the art of Micro-CT applications in dental research. *Int J Oral Sci* 1: 177–188. https://doi.org/10.4248/ijos09031

29. Lauren B, Pedro T, Felix G, et al. (2021) Assessment of trabecular bone during dental implant planning using cone-beam computed tomography with high-resolution parameters. *TODENTJ* 2021: 15–57. https://doi.org/10.2174/1874210602115010057
30. Zhang G, Pan XH, Liu Z, et al. (2011) Impaired bone healing pattern in mice with ovariectomy-induced osteoporosis: a drill-hole defect model. *Bone* 48: 1388–1400. https://doi.org/10.1016/j.bone.2011.03.720
31. Parsa A, Ibrahim N, Hassan B, et al. (2015) Bone quality evaluation at dental implant site using multislice CT, micro-CT, and cone beam CT. *Clin Oral Implants Res* 26: e1–7. https://doi.org/10.1111/clr.12315
32. Calvo Guirado JL, Ortiz Ruiz AJ, Gomez Moreno G, et al. (2008) Immediate loading and immediate restoration in 105 expanded-platform implants via the diem system after a 16-month follow-up period. *Med Oral Patol Oral Cir Bucal* 13: E576–581. https://pubmed.ncbi.nlm.nih.gov/18758403
33. Enriquez-Sacristan C, Barona-Dorado C, Calvo-Guirado JL, et al. (2011) Immediate post-extraction implants subject to immediate loading: a meta-analytic study. *Med Oral Patol Oral Cir Bucal* 16: e919–924. https://doi.org/10.4317/medoral.16918
34. Balbinot GS, Leitune VCB, Ponzoni D, et al. (2019) Bone healing with niobium-containing bioactive glass composition in rat femur model: a micro-CT study. *Dent Mater* 35: 1490–1497. https://doi.org/10.1016/j.dental.2019.07.012
35. Jiang Y, Zhao J, Liao EY, et al. (2005) Application of micro-CT assessment of 3-D bone micro-structure in preclinical and clinical studies. J *Bone Miner Metab* 23: 122–131. https://doi.org/10.1007/bf03026336
36. Van Dessel J, Nicolielo LF, HuangY, et al. (2017) Accuracy and reliability of different cone beam computed tomography (CBCT) devices for structural analysis of alveolar bone in comparison with multislice CT and micro-CT. *Eur J Oral Implantol* 10: 95–105. https://pubmed.ncbi.nlm.nih.gov/28327698
37. Cano J, Campo J, Vaquero JJ, et al. (2008) High resolution image in bone biology II. Review of the literature. *Med Oral Patol Oral Cir Bucal* 13: E31–E35. https://pubmed.ncbi.nlm.nih.gov/18167477
38. Tjong W, Nirody J, Burghardt AJ, et al. (2014) Structural analysis of cortical porosity applied to HR-pQCT data. *Med Phys.* 41: 013701. https://doi.org/10.1118/1.4851575
39. Rabelo GD, Coutinho-Camillo C, Kowalski LP, et al. (2017). Evaluation of cortical mandibular bone in patients with oral squamous cell carcinoma. *Clin Oral Investig* 22: 783–790. https://doi.org/10.1007/s00784-017-2153-8
40. Blok Y, Gravesteijn F, van Ruijven L, et al. (2013) Micro-architecture and mineralization of the human alveolar bone obtained with microCT. *Arch Oral Biol* 58: 621–627. https://doi.org/10.1016/j.archoralbio.2012.10.001
41. Romao M, Marques M, Cortes A, et al. (2015) Micro-computed tomography and histomorphometric analysis of human alveolar bone repair induced by laser phototherapy: a pilot study. *Int J Oral Maxillofac Surg* 44: 1521–1528. https://doi.org/10.1016/j.ijom.2015.08.989
42. Norton MR and Gamble C (2001) Bone classification: an objective scale of bone density using the computerized tomography scan. *Clin Oral Implant Res* 12: 79–84. https://doi.org/10.1034/j.1600-0501.2001.012001079.x

43. Annunziata M and Guida L (2015) The effect of titanium surface modifications on dental implant osseointegration. *Craniofacial Sutures* 17: 62–77. https://doi.org/10.1159/000381694
44. Junker R, Dimakis A, Thoneick M, et al. (2009) Effects of implant surface coatings and composition on bone integration: a systematic review. *Clin Oral Implant Res* 20: 185–206. https://doi.org/10.1111/j.1600-0501.2009.01777.x
45. Chavez MB, Chu EY, Kram V, et al. (2021) Guidelines for micro-computed tomography analysis of rodent dentoalveolar tissues. *JBMR Plus* 5: e10474. https://doi.org/10.1002/jbm4.10474
46. Molly L (2006) Bone density and primary stability in implant therapy. *Clin Oral Implant Res* 17: 124–135. https://doi.org/10.1111/j.1600-0501.2006.01356.x
47. De Smet E, Jaecques S, Wevers M, et al. (2006) Effect of controlled early implant loading on bone healing and bone mass in guinea pigs, as assessed by micro-CT and histology. *Eur J Oral Sci* 114: 232–242. https://doi.org/10.1111/j.1600-0722.2006.00355.x
48. Barrett JF and Keat N (2004) Artifacts in CT: recognition and avoidance. *Radiographics* 24: 1679–1691. https://doi.org/10.1148/rg.246045065
49. Rebaudi A, Trisi P, Cella R, et al. (2010) Preoperative evaluation of bone quality and bone density using a novel CT/microCT based hard-normal-soft classification system. *Int J Oral Maxillofac Implants* 25: 75–85. https://pubmed.ncbi.nlm.nih.gov/20209189
50. Rebaudi A, Koller B, Laib A, et al. (2004) Microcomputed tomographic analysis of the peri-implant bone. *Int J Periodontics Restor Dent* 24: 316–325. https://pubmed.ncbi.nlm.nih.gov/15446401
51. Song JW, Cha JY, Bechtold TE, et al. (2004) Influence of peri-implant artifacts on bone morphometric analysis with microcomputed tomography. *Int J Oral Maxillofac Implant*s 28: 519–525. https://doi.org/10.11607/jomi.1632

AIMS Press